

This document is confidential and is proprietary to the American Chemical Society and its authors. Do not copy or disclose without written permission. If you have received this item in error, notify the sender and delete all copies.

## Improved Alchemical Free Energy Calculations with Optimized Smoothstep Softcore Potentials

Journal:	<i>Journal of Chemical Theory and Computation</i>
Manuscript ID	ct-2020-00237p
Manuscript Type:	Article
Date Submitted by the Author:	10-Mar-2020
Complete List of Authors:	Lee, Tai-sung; Rutgers, the State University of New Jersey, Laboratory for Biomolecular Simulation Research, and Department of Chemistry and Chemical Biology Lin, Zhixiong; Silicon Therapeutics Allen, Bryce; Silicon Therapeutics, Lin, Charles; Silicon Therapeutics Radak, Brian; Argonne National Laboratory, Silicon Therapeutics, LLC Tao, Yujun; Rutgers The State University of New Jersey, Department of Chemistry and Chemical Biology Tsai, Hsu-Chun; Rutgers, the State University of New Jersey, Laboratory for Biomolecular Simulation Research, and Department of Chemistry and Chemical Biology Sherman, Woody; Silicon Therapeutics, York, Darrin; Rutgers, the State University of New Jersey, Laboratory for Biomolecular Simulation Research, and Department of Chemistry and Chemical Biology

SCHOLARONE™  
Manuscripts

1  
2  
3  
4  
5  
6  
7  
8  
9  
10  
11  
12  
13 **Improved Alchemical Free Energy Calculations**  
14  
15  
16 **with Optimized Smoothstep Softcore Potentials**  
17  
18  
19  
20  
21  
22

23 Tai-Sung Lee,<sup>†</sup> Zhixiong Lin,<sup>‡</sup> Bryce K. Allen,<sup>‡</sup> Charles Lin,<sup>‡</sup> Brian K. Radak,<sup>‡</sup>  
24  
25 Yujun Tao,<sup>†</sup> Hsu-Chun Tsai,<sup>†</sup> Woody Sherman,<sup>‡</sup> and Darrin M. York<sup>\*,†</sup>  
26  
27  
28

29 <sup>†</sup>*Laboratory for Biomolecular Simulation Research, Institute for Quantitative Biomedicine*  
30 *and Department of Chemistry and Chemical Biology, Rutgers University, Piscataway, NJ*  
31 *08854, USA*  
32  
33

34  
35 <sup>‡</sup>*Silicon Therapeutics LLC, Boston, MA 02111, USA*  
36  
37

38 E-mail: Darrin.York@rutgers.edu  
39  
40  
41  
42  
43  
44  
45  
46  
47  
48  
49  
50  
51  
52  
53  
54  
55  
56  
57  
58  
59  
60

## Abstract

Progress in the development of GPU-accelerated free energy simulation software has enabled practical applications on complex biological systems and fueled efforts to develop more accurate and robust predictive methods. In particular, this work re-examines concerted (a.k.a., single-step or unified) alchemical transformations commonly used in the prediction of hydration and relative binding free energies (RBFE). We first classify several known challenges in these calculations into three categories: endpoint catastrophes, particle collapse, and large gradient-jumps. While endpoint catastrophes have long been resolved using softcore potentials, the remaining two problems occur much more sporadically and can result in either numerical instability (i.e. complete failure of a simulation) or inconsistent estimation (i.e. stochastic convergence to an incorrect result). The particle collapse problem stems from an imbalance in short-range electrostatic and repulsive interactions and can, in principle, be solved by appropriately balancing the respective softcore parameters. However, the large gradient-jump problem itself arises from the sensitivity of the free energy to large values of the softcore parameters, as might be used in trying to solve the particle collapse issue. Often no satisfactory compromise exists with the existing softcore potential form. As a framework for solving these problems, we developed a new family of smoothstep softcore (SSC) potentials motivated by an analysis of the derivatives along the alchemical path. The smoothstep polynomials generalize the monomial functions that are used in most implementations and provide an additional path-dependent smoothing parameter. The effectiveness of this approach is demonstrated on simple, yet pathological cases that illustrate the three problems outlined. With appropriate parameter selection we find that a second-order SSC(2) potential does at least as well as the conventional approach and provides a vast improvement in terms of consistency across all cases. Lastly, we compare the concerted SSC(2) approach against the gold-standard stepwise (a.k.a., decoupled or multi-step) scheme over a large set of RBFE calculations as might be encountered in drug discovery.

## Introduction

Recent progress and improvements in computer hardware, simulation software, and free energy methods,<sup>1-12</sup> especially the development of highly efficient and cost-effective GPU accelerated free energy calculations,<sup>12-18</sup> have significantly extended the accessible timescales of computer simulations and scope of applications. In addition to ongoing challenges of developing more accurate force fields and efficient sampling methods, there is need to improve our ability to optimally set up alchemical free energy calculations.<sup>19-30</sup>

The setup problem refers to not only how to create the relevant necessary input files but also the proper simulation protocols and parameters that will yield the best results for a given system of interest. In alchemical free energy simulations, one of the most difficult but pivotal technical issues is the choice of the alchemical path connecting the two real states (i.e., connecting the two thermodynamic endpoints). While, the free energy difference between two states is independent of the path that connects them in the regime of complete conformational sampling, in practical calculations of complex systems, the choice of the alchemical transformation path is critical to obtain stable, converged results with affordable sampling.

One of the first major obstacles that was encountered in simple concerted (a.k.a., single-step or unified) linear alchemical transformations was the "endpoint catastrophe".<sup>31-37</sup> The endpoint catastrophe occurs when the potential energy of one real end state needs to be evaluated with the conformational ensemble generated from the other real end state in order to obtain exponentiated energy differences or thermodynamic derivatives required to obtain the free energy difference.<sup>32-34</sup> Since different atoms in the two states can be artificially superimposed in such a transformation, this can lead to energy differences or thermodynamic derivatives that are unstably large in magnitude, and even singular. The singularity arises due to "hard" exchange repulsions and/or Coulombic interactions between atoms in the core transformation region that unphysically overlap.<sup>33</sup>

There are two general approaches to address the endpoint catastrophe. The first is

1  
2  
3 the use of “softcore potentials” with separation-shifted scaling,<sup>34,36</sup> short-range switching,<sup>37</sup>  
4 or capping the short-range interactions.<sup>38</sup> The second is to use non-linear mixing of the  
5 endpoint potentials.<sup>31–33,35,39</sup> Nowadays combinations of these two approaches are most often  
6 utilized.<sup>36,38,39</sup> A formalism for minimal variance path based on the standard form of softcore  
7 potentials has also been reported.<sup>40,41</sup> These have been successful strategies to formally  
8 address the classical endpoint catastrophe, as defined in the present context.

9  
10  
11  
12  
13  
14  
15 Nonetheless, with the use of softcore potentials to address the endpoint catastrophe, there  
16 remains two other major problems in concerted transformations that can result in numerical  
17 instabilities and poor statistical results.<sup>37</sup> The first is the “particle collapse” problem that  
18 stems from an imbalance of softcore Coulomb attraction and exchange repulsions, and can  
19 lead to artificial minima where particles from the two transforming states are on top of one  
20 another. The second is the “large gradient-jump” problem that arises from sensitivity of  
21 the free energy to large values of the softcore parameters sometimes required to balance the  
22 softcore Coulomb and exchange interactions.

23  
24  
25  
26  
27  
28  
29  
30  
31 An alternate strategy to circumvent the “particle collapse” and “large gradient-jump”  
32 problems altogether is to avoid use of a concerted transformation, and instead use a “step-  
33 wise” approach, sometimes referred to as “multi-step” or “split” procedures,<sup>42</sup> in which the  
34 electrostatic and Lennard-Jones (LJ) interactions are handled in separate steps in the al-  
35 chemical transformation. An example of a stepwise “decharge-vdW-recharge” strategy would  
36 be as follows.

- 37  
38  
39  
40  
41  
42  
43 • Step 1: de-charge the mutating atoms in the initial state (with LJ and other parameters  
44 fixed at their initial state values) so that there will be no electrostatic interactions that  
45 can lead to an imbalance in the next step. Note, during this step, all interactions  
46 including electrostatics from the final state are turned off.
- 47  
48  
49  
50  
51  
52 • Step 2: with all the mutating atoms in both the initial and final states turned off (i.e.,  
53 “decharged”), transform the LJ parameters, including  $r^{-12}$  exchange repulsions, from  
54 the initial state to the final state, along with any additional bonded parameters.

- Step 3: re-charge the mutating atoms (with LJ and other parameters fixed at their final state values) to their final state values.

While stepwise approaches have been demonstrated to be quite robust, they have several disadvantages. First, the procedure is more tedious to set up and can be sensitive to the choice of atoms in the decharge/recharge region, in some cases leading to intermediate states that have significantly different net charge. Second, the procedure is more computationally intensive as it requires more steps, each with different sampling requirements and statistical error estimates. And third, the procedure is not well suited for advanced  $\lambda$ -schedule optimization and enhanced sampling schemes, such as  $\lambda$  dynamics,<sup>43–46</sup> Hamiltonian replica exchange methods,<sup>47–51</sup> adaptive biasing<sup>44,52,53</sup> or self-adjusted mixture sampling<sup>54,55</sup> methods. Consequently, it is of practical interest to work toward a more robust and efficient solution for concerted alchemical transformations.

In this work, we present methods for improved “concerted” alchemical free energy transformations of complex biomolecular systems. The remainder of the paper is outlined as follows. The Theory section develops the mathematical model framework, provides definitions of the three main problems commonly encountered in concerted transformations, and presents a systematic set of formulas to facilitate their discussion. We then formulate a new smooth softcore potential using smoothstep functions of variable order  $P$  that we designate “SSC( $P$ )”. In the Results section, we demonstrate how the SSC(2) potential with optimized parameters is able to overcome all problematic cases of concerted alchemical transformations we have yet encountered. We demonstrate the robustness of the SSC(2) potential compared to a conventional widely used softcore potential for a broad range of hydration free energies and RBFEE calculations. Results are compared to benchmark quality “stepwise” (decharge-vdW-recharge) free energy calculations. The Discussion places the work into broader context, and the Conclusion summarizes the main points of the paper and identifies future research directions. The methods presented here have been implemented as a modified enhancement of the GPU-accelerated free energy methods in AMBER18,<sup>17</sup> and will be forthcoming in the

1  
2  
3 AMBER20 release.  
4  
5  
6  
7  
8  
9  
10  
11  
12  
13  
14  
15  
16  
17  
18  
19  
20  
21  
22  
23  
24  
25  
26  
27  
28  
29  
30  
31  
32  
33  
34  
35  
36  
37  
38  
39  
40  
41  
42  
43  
44  
45  
46  
47  
48  
49  
50  
51  
52  
53  
54  
55  
56  
57  
58  
59  
60

## Theory

One can formulate the computation of relative free energies from equilibrium simulations using a thermodynamic perturbation (TP)<sup>56</sup> (sometimes referred to as “free energy perturbation”) or thermodynamic integration (TI),<sup>57,58</sup> or through non-equilibrium ensemble simulations using the Jarzynski equality and its equation variations.<sup>59–64</sup> In the present work, we focus on equilibrium methods, and formulate the problem in the TI framework. Nonetheless, the fundamental barriers to progress that we address herein are not specific to the TI method, as we show through numerical examples, the new methods presented here are equally transferable to TP methods with Bennett Acceptance Ratio (BAR) analysis and its multistate variant (MBAR).<sup>65–69</sup>

### Thermodynamic Integration with Original AMBER Softcore Potentials

The free energy is a state function, and thus the free energy difference between thermodynamic states is independent of the path that connects them (assuming fully converged sampling along the path). Computationally, however, the choice of this pathway is most often of immense importance, as for non-trivial problems, statistical sampling is required not just at the end states, but along the pathway itself.

Consider the transformation of a system of  $N$  particles in an initial state “0” characterized by potential energy function  $U_0(\mathbf{q})$ , where  $\mathbf{q}$  represent the degrees of freedom of the system (e.g., Cartesian positions of each particle along with any system variables), to a final state “1” characterized by potential energy function  $U_1(\mathbf{q})$  having the same degrees of freedom. Let us define a thermodynamic parameter  $\lambda$  that smoothly connects these states through a  $\lambda$ -dependent potential  $U(\mathbf{q}; \lambda)$  such that  $U(\mathbf{q}; 0) = U_0(\mathbf{q})$  and  $U(\mathbf{q}; 1) = U_1(\mathbf{q})$ . In this case, the change in free energy  $\Delta G_{0 \rightarrow 1} = G_1 - G_0$  can be determined through the thermodynamic



1  
2  
3 integration formula  
4  
5

$$\Delta G_{0 \rightarrow 1} = \int_0^1 d\lambda \left\langle \frac{dU(\mathbf{q}; \lambda)}{d\lambda} \right\rangle_{\lambda} \approx \sum_{k=1}^M w_k \left\langle \frac{dU(\mathbf{q}; \lambda)}{d\lambda} \right\rangle_{\lambda_k} \quad (1)$$

6  
7  
8  
9  
10 where the second sum indicates numerical integration over  $M$  quadrature points ( $\lambda_k$ , for  
11  
12  $k = 1, \dots, M$ ) with associated weights  $w_k$ . We now discuss specific ways in which the  $U(\mathbf{q}; \lambda)$   
13  
14 can be constructed. The simplest way to establish a thermodynamic connection is to use a  
15  
16 linear interpolation between states, which we will designate as  $U^L(\mathbf{q}; \lambda)$ :  
17  
18

$$U^L(\mathbf{q}; \lambda) = (1 - \lambda)U_0(\mathbf{q}) + \lambda U_1(\mathbf{q}) = U_0(\mathbf{q}) + \lambda \Delta U(\mathbf{q}) \quad (2)$$

19  
20  
21 where  $\Delta U(\mathbf{q}) = U_1(\mathbf{q}) - U_0(\mathbf{q})$ . The simple linear alchemical transformation pathway has  
22  
23 the thermodynamic derivative  
24  
25  
26

$$\frac{dU^L(\mathbf{q}; \lambda)}{d\lambda} = U_1(\mathbf{q}) - U_0(\mathbf{q}) = \Delta U(\mathbf{q}) \quad (3)$$

27  
28  
29 Hence, the common energy components that are identical between  $U_1(\mathbf{q})$  and  $U_0(\mathbf{q})$  need not  
30  
31 be explicitly considered as the corresponding difference is zero. As has been well established  
32  
33 and is discussed in more detail below, however, the linear alchemical transformation pathway  
34  
35 leads to practical problems that can be partially overcome by the use of so-called “softcore”  
36  
37 potentials. These potentials, in the present context and the discussion that follows, apply  
38  
39 only to non-bonded (i.e., LJ and electrostatic) interactions within the non-bonded cut-off.<sup>34,36</sup>  
40  
41 All other components of the energy are achieved here through the conventional linear trans-  
42  
43 formation pathway, although other non-linear pathways are also possible through parameter  
44  
45 interpolation.<sup>16</sup> Here we define the original softcore potential transformation pathway<sup>36</sup> in  
46  
47 AMBER as  
48  
49  
50  
51  
52  
53

$$U^{SC}(\mathbf{q}; \lambda) = (1 - \lambda)U_0^{SC}(\mathbf{q}; \lambda) + \lambda U_1^{SC}(\mathbf{q}; 1 - \lambda) = U_0^{SC}(\mathbf{q}; \lambda) + \lambda \Delta U^{SC}(\mathbf{q}; \lambda) \quad (4)$$

where  $\Delta U^{SC}(\mathbf{q}; \lambda) \equiv U_1^{SC}(\mathbf{q}; 1 - \lambda) - U_0^{SC}(\mathbf{q}; \lambda)$ , and the thermodynamic derivative is given by

$$\begin{aligned} \frac{dU^{SC}(\mathbf{q}; \lambda)}{d\lambda} &= [U_1^{SC}(\mathbf{q}; 1 - \lambda) - U_0^{SC}(\mathbf{q}; \lambda)] \\ &+ \left[ (1 - \lambda) \left( \frac{dU_0^{SC}(\mathbf{q}; \lambda)}{d\lambda} \right) + \lambda \left( \frac{dU_1^{SC}(\mathbf{q}; 1 - \lambda)}{d\lambda} \right) \right] \end{aligned} \quad (5)$$

In the current AMBER implementation, a nonbonded cut-off is defined and the softcore potentials are applied as correction terms to the original non-bonded LJ and electrostatic interactions between the softcore region atoms and other non-softcore atoms within the nonbonded cut-off. As a result, when utilizing the particle-mesh Ewald method (PME),<sup>70</sup> only the direct space term evaluated within the nonbonded cut-off is affected by the softcore potentials.

There have been many different proposed softcore potential forms that modify, or “soften”, these interactions. The LJ and electrostatic interactions for a set of interacting point particles  $i$  and  $j$  separated by a distance  $r_{ij}$  are given by

$$U_{LJ}(r_{ij}) = 4\epsilon_{ij} \left[ \left( \frac{\sigma_{ij}}{r_{ij}} \right)^{12} - \left( \frac{\sigma_{ij}}{r_{ij}} \right)^6 \right] \quad (6)$$

and

$$U_C(r_{ij}) = \left( \frac{q_i q_j}{4\pi\epsilon_0} \right) \frac{1}{r_{ij}} \quad (7)$$

where  $\sigma_{ij}$  and  $\epsilon_{ij}$  are the pairwise van der Waals contact distance and well depth, respectively, and  $q_i$  and  $q_j$  are the partial charges of particles  $i$  and  $j$ .

The Cartesian derivatives of these energies are straight forward as  $\nabla_i U(r_{ij}) = (\mathbf{r}_{ij}/r_{ij})(dU/dr_{ij}) = -\nabla_j U(r_{ij})$ , where the derivatives with respect to  $r_{ij}$  are given by

$$\frac{dU_{LJ}(r_{ij})}{dr_{ij}} = -4 \left( \frac{\epsilon_{ij}}{r_{ij}} \right) \left[ 12 \left( \frac{\sigma_{ij}}{r_{ij}} \right)^{12} - 6 \left( \frac{\sigma_{ij}}{r_{ij}} \right)^6 \right] \quad (8)$$

1  
2  
3 and

$$\frac{dU_C(r_{ij})}{dr_{ij}} = - \left( \frac{q_i q_j}{4\pi\epsilon_0} \right) \frac{1}{r_{ij}^2} \quad (9)$$

4  
5  
6  
7  
8 These derivatives are programmed in molecular simulation software codes in order to derive  
9 the normal electrostatic and van der Waals forces on particles. In order to “soften” these  
10 pairwise interactions with particles contained within the selected softcore region, one can  
11 modify the effective interaction distance by introducing a parametric form for separation-  
12 shifted scaling with an adjustable parameter. A commonly used form of these modifications  
13 is<sup>34,36</sup>

$$r_{ij}^{\text{LJ}}(\lambda; \alpha) = [r_{ij}^n + \lambda\alpha\sigma_{ij}^n]^{1/n} \quad (10)$$

14  
15  
16  
17  
18  
19 and

$$r_{ij}^{\text{C}}(\lambda; \beta) = [r_{ij}^m + \lambda\beta]^{1/m} \quad (11)$$

20  
21  
22  
23  
24  
25  
26  
27  
28 where  $n$  and  $m$  are positive integers and  $\alpha$  and  $\beta$  are adjustable positive semidefinite pa-  
29 rameters for the LJ and electrostatic softcore interactions, respectively, with values of zero  
30 corresponding to no softcore modification for any  $\lambda$  value. In several molecular simulation  
31 software suites, including the default in AMBER, the values of  $n = 6$  and  $m = 2$  are used,  
32 although other values have also been suggested.<sup>36</sup> Note that for positive values of  $\alpha$  and  
33  $\beta$  parameters and  $\lambda$  values between 0 and 1, the effective interaction distances satisfy the  
34 conditions

$$r_{ij}^{\text{LJ}}(\lambda; \alpha) \geq r_{ij} \quad (12)$$

$$r_{ij}^{\text{C}}(\lambda; \beta) \geq r_{ij} \quad (13)$$

35  
36  
37  
38  
39  
40  
41  
42  
43  
44  
45  
46  
47  
48 where the equality holds only for the real state endpoint  $\lambda=0$ . This results in a “softening”  
49 of the LJ and electrostatic interactions with increasing values of  $\alpha$  and  $\beta$  parameters, respec-  
50 tively, particularly at short range where they are largest in magnitude. From these modified  
51  
52  
53  
54  
55  
56  
57  
58  
59  
60

effective interaction distances, the LJ and electrostatic softcore potentials can be defined as

$$U_{\text{LJ}}^{\text{SC}}(r_{ij}; \lambda) = U_{\text{LJ}} [r_{ij}^{\text{LJ}}(\lambda; \alpha)] \quad (14)$$

and

$$U_{\text{C}}^{\text{SC}}(r_{ij}; \lambda) = U_{\text{C}} [r_{ij}^{\text{C}}(\lambda; \beta)] \quad (15)$$

The thermodynamic derivatives with respect to  $\lambda$  can be obtained using the chain relation as

$$\frac{dU_{\text{LJ}}^{\text{SC}}(r_{ij}; \lambda)}{d\lambda} = \frac{dU_{\text{LJ}} [r_{ij}^{\text{LJ}}(\lambda; \alpha)]}{dr_{ij}^{\text{LJ}}(\lambda; \alpha)} \cdot \frac{dr_{ij}^{\text{LJ}}(\lambda; \alpha)}{d\lambda} \quad (16)$$

where

$$\frac{dr_{ij}^{\text{LJ}}(\lambda; \alpha)}{d\lambda} = (\alpha/n) \cdot \sigma_{ij}^n \cdot [r_{ij}^{\text{LJ}}(\lambda; \alpha)]^{(1-n)/n} \quad (17)$$

and

$$\frac{dU_{\text{C}}^{\text{SC}}(r_{ij}; \lambda)}{d\lambda} = \frac{dU_{\text{C}} [r_{ij}^{\text{C}}(\lambda; \beta)]}{dr_{ij}^{\text{C}}(\lambda; \beta)} \cdot \frac{dr_{ij}^{\text{C}}(\lambda; \beta)}{d\lambda} \quad (18)$$

where

$$\frac{dr_{ij}^{\text{C}}(\lambda; \beta)}{d\lambda} = (\beta/m) \cdot [r_{ij}^{\text{C}}(\lambda; \beta)]^{(1-m)/m} \quad (19)$$

## Problems with Original AMBER Softcore Potentials and Their Underlying Causes

The field of free energy methods is vast, and yet there currently exists no commonly accepted and consistently used terminology that enables discussion of certain classes of problems that can occur when performing free energy simulations. Here we define the main problems that we have encountered regarding the alchemical transformation path in free energy simulations and have endeavored to overcome in the current work. Further, we distinguish the problems themselves, which manifest as observed symptoms in the simulations, from their underlying origins (causes), which we relate mathematically to the equations, in order to motivate their

1  
2  
3 solutions.

4  
5 There are three main problems related to the alchemical path and associated softcore  
6 potential that can commonly occur in free energy simulations, and in particular with so-  
7 called “concerted transformations” that involve simultaneous changes in both non-bonded  
8 LJ and electrostatic terms. We will refer to these as the endpoint catastrophe, the particle  
9 collapse problem, and the large gradient-jump problem. We now discuss each of these in  
10 more detail, including defining the symptoms of each problem, highlighting their underlying  
11 causes, and outlining solutions.  
12  
13  
14  
15  
16  
17  
18

### 19 1. Endpoint catastrophe:

20  
21 *Definition:* With linear alchemical transformations, the sharp divergence (and sometimes  
22 singularity) of the contribution to the free energy at the thermodynamic endpoints ( $\lambda$  values  
23 near 0 and 1).  
24  
25  
26

27 *Cause:* endpoint catastrophes are due to poor phase space overlap. The endpoint catastro-  
28 phe is a well known problem often encountered with simple linear alchemical transformations  
29 where the total potential is defined as the linear combinations of the end state potentials,  
30 and occurs when the  $\lambda$  value approaches a real state endpoint where the potential energy of  
31 one real state endpoint needs to be evaluated with the conformational ensemble generated  
32 from the other real state endpoint, and can result in unphysical atom-atom overlap and  
33 thermodynamic derivatives. Equation (3) shows that the required thermodynamic deriva-  
34 tive involves a difference between real state endpoint potentials (i.e.,  $\Delta U(\mathbf{q})$ ) for *all*  $\lambda$  points,  
35 even if this difference is unstably large.  
36  
37  
38  
39  
40  
41  
42  
43  
44

45 *Solution:* the endpoint catastrophe can be avoided by the use of original AMBER soft-  
46 core potentials. Formally, the endpoint catastrophe can be avoided by use of the softcore  
47 potentials presented in Equation (4), with particular sensitivity to the  $\alpha$  parameter that  
48 tunes the “softness” of the LJ terms, including the short-ranged repulsive potential. Larger  
49  $\beta$  and especially  $\alpha$  values thus tend to have the greatest affect in alleviating the endpoint  
50 catastrophe.  
51  
52  
53  
54  
55  
56  
57  
58  
59  
60

## 2. Particle collapse:

*Definition:* With softcore potentials, the artificial superposition of particles at intermediate values of  $\lambda$  that can lead to large amplitude fluctuations or phase transition behavior along the  $\lambda$  dimension.<sup>38</sup>

*Cause:* *particle collapse results from an imbalance of Coulomb attraction and exchange repulsions that favors atomic overlap.* While softcore potentials formally eliminate singularities at the endpoints, they can also lead to the creation of new artificial minima at  $r = 0$  if the short-range exchange repulsion terms of the softcore LJ potential is not sufficient to overcome the softcore Coulomb attractions of oppositely charged particles.<sup>36,37</sup> This could cause unwanted alchemical traps, or even phase transition-like behavior, along the  $\lambda$  dimension, resulting in unstable, unconverged numerical results.

*Solution:* *the Coulomb-Exchange imbalance problem can be overcome by adjustment (decrease) of the  $\alpha/\beta$  softcore parameter ratio, and/or modification of the softcore potential functional form.* In order to avoid Coulomb-Exchange imbalance, the softcore exchange repulsions need to be made “harder” (smaller  $\alpha$  value) and/or the softcore Coulomb interactions need to be made “softer” (larger  $\beta$  value). While this adjustment is somewhat system-dependent, as will be illustrated below, certain combinations appear to be remarkably robust for a variety of transformations in different environments for a range of protein-ligand systems.

## 3. Large gradient-jump:

*Definition:* With softcore potentials, the sensitivity of the free energy for large values of the softcore parameters can lead to spurious jumps in the free energy near the thermodynamic endpoints.

*Cause:* *large jumps in free energy can result from sensitivity of the thermodynamic derivatives (gradient) to certain softcore parameter values near the real state endpoints.* This is particularly manifested when large  $\beta$  values are required to adjust the  $\alpha/\beta$  softcore parameter ratio to solve the Coulomb-Exchange imbalance problem. This can result in an dramatic

1  
2  
3 increase in the terms in Equation (5) involving  $\lambda$  derivatives of  $U_1^{SC}$  and  $U_0^{SC}$  at the  $\lambda=1$  and  
4  
5 0 endpoints, respectively. Equations (17) and (19) show that the thermodynamic derivatives  
6  
7 for the softcore LJ and Coulomb interactions are roughly linear in the parameters  $\alpha$  and  $\beta$ ,  
8  
9 respectively, particularly for  $\lambda$  values near the real state endpoints where energy changes are  
10  
11 typically largest and nonlinear.<sup>37</sup>  
12

13 *Solution: the large gradient-jump problem can be solved by formulating a more sophis-*  
14 *ticated smooth softcore potential that has derivatives that vanish at the endpoints.* We for-  
15  
16 mulate a family of smooth softcore potentials that use smoothstep weighting functions with  
17  
18 favorable endpoint derivative properties with the intent of developing and testing a robust  
19  
20 softcore framework that can be used for efficient concerted transformations. With proper  
21  
22 choice of  $\alpha$  and  $\beta$  softcore parameters, together with an appropriately smooth weighting  
23  
24 function (see below), we find a solution across all the above problems for a wide range of  
25  
26 alchemical transformations, including several severe problematic test cases.  
27  
28  
29  
30  
31  
32  
33  
34  
35  
36  
37  
38  
39  
40  
41  
42  
43  
44  
45  
46  
47  
48  
49  
50  
51  
52  
53  
54  
55  
56  
57  
58  
59  
60

## Formulation of a family of smoothstep softcore potentials for robust concerted alchemical transformations

We consider a family of smoothstep functions,  $S_P(\lambda)$ , of orders  $P$  ( $P = 0, 1, 2, \dots$ ) and are defined as the polynomial functions (up to  $P = 4$  shown):

for  $0 \leq x \leq 1$  :

$$S_0(x) = x,$$

$$S_1(x) = -2x^3 + 3x^2,$$

$$S_2(x) = 6x^5 - 15x^4 + 10x^3,$$

$$S_3(x) = -20x^7 + 70x^6 - 84x^5 + 35x^4,$$

$$S_4(x) = 70x^9 - 315x^8 + 540x^7 - 420x^6 + 126x^5,$$

and

$$S_P(x < 0) = 0; S_P(x > 1) = 1, \forall P \in \mathbb{N} \quad (20)$$

The smoothstep functions are monotonically increasing functions that have the desirable endpoint values:

$$S_P(0) = 0; S_P(1) = 1 \quad \forall P \in \mathbb{N} \quad (21)$$

and derivative properties

$$\left[ \frac{d^k S_P(x)}{dx^k} \right]_{x=0} = \left[ \frac{d^k S_P(x)}{dx^k} \right]_{x=1} = 0 \quad \forall k \in \mathbb{N}, \quad 0 < k \leq P \quad (22)$$

From these smoothstep functions, we create a family of smooth softcore potentials for nonbonded LJ and electrostatic interactions involving atoms in the softcore region by re-



placing  $\lambda$  with  $S_P(\lambda)$  in Equations (4) and (5) to obtain:

$$\begin{aligned} U^{\text{SSC}(P)}(\mathbf{q}; \lambda) &= U^{SC}[\mathbf{q}; S_P(\lambda)] \\ &= [1 - S_P(\lambda)] \cdot U_0^{SC}[\mathbf{q}; S_P(\lambda)] + S_P(\lambda) \cdot U_1^{SC}[\mathbf{q}; 1 - S_P(\lambda)] \end{aligned} \quad (23)$$

with thermodynamic derivatives

$$\frac{dU^{\text{SSC}(P)}(\mathbf{q}; \lambda)}{d\lambda} = \frac{dU^{SC}[\mathbf{q}; S_P(\lambda)]}{dS_P(\lambda)} \cdot \frac{dS_P(\lambda)}{d\lambda} \quad (24)$$

where, following from Equation (5), we have

$$\begin{aligned} \frac{dU^{SC}[\mathbf{q}; S_P(\lambda)]}{dS_P(\lambda)} &= \{U_1^{SC}[\mathbf{q}; 1 - S_P(\lambda)] - U_0^{SC}[\mathbf{q}; S_P(\lambda)]\} \\ &+ \left\{ [1 - S_P(\lambda)] \cdot \frac{dU_0^{SC}[\mathbf{q}; S_P(\lambda)]}{dS_P(\lambda)} + S_P(\lambda) \cdot \frac{dU_1^{SC}[\mathbf{q}; 1 - S_P(\lambda)]}{dS_P(\lambda)} \right\} \end{aligned} \quad (25)$$

Note that Equation (23) for  $U^{\text{SSC}(P)}(\mathbf{q}; \lambda)$  is identical to Equation (4) for  $U^{SC}(\mathbf{q}; \lambda)$  with the latter having  $\lambda$  argument replaced by  $S_P(\lambda)$ . Further, note that  $U^{\text{SSC}(0)}(\mathbf{q}; \lambda)$  ( $P = 0$  family member), is identical to  $U^{SC}(\mathbf{q}; \lambda)$ . Thus the original softcore potential is contained as the lowest order member of the smoothstep softcore potential family described here. However, this is the only member of the family that does not have derivative values that vanish at the boundaries ( $\lambda=0$  and 1), but rather has a constant value of 1 over the range of  $\lambda$ . As we will demonstrate below, other higher-order members of the family have numerical properties that are much more well-behaved, and in particular the  $S_2$  family member, with appropriate choice of  $\alpha$  and  $\beta$  values overcomes all problematic cases of concerted transformations.

As mentioned earlier, the smoothstep softcore potential introduced here is only applied to nonbonded LJ and electrostatic interactions involving between atoms in the softcore region and atoms in the non-softcore region within the cutoff. To be consistent, the smoothstep combination scheme of potentials (the prefactors  $1 - S_P(\lambda)$  and  $S_P(\lambda)$  in Equation (23)) is applied to not only the above softcore terms but also to the corresponding the long-range

1  
2  
3 analytic dispersion "tail" corrections<sup>71</sup> beyond the cut-off, and 1-4 scaled non-bonded terms.  
4  
5 Other components of the  $\lambda$ -dependent potential energy without softcore potential correction,  
6  
7 and their thermodynamic derivatives do not use the smoothstep functions but use the original  
8  
9 linear combination scheme. These terms include the PME reciprocal space term (including  
10  
11 the "self-energy" and net charge correction), bonded terms, and restraint terms.  
12  
13  
14  
15  
16  
17  
18  
19  
20  
21  
22  
23  
24  
25  
26  
27  
28  
29  
30  
31  
32  
33  
34  
35  
36  
37  
38  
39  
40  
41  
42  
43  
44  
45  
46  
47  
48  
49  
50  
51  
52  
53  
54  
55  
56  
57  
58  
59  
60

# Methods

## Simulation setup and protocols

A modified version of AMBER18 with the proposed SSC(P) scheme implementation, forthcoming in AMBER20, was employed for all simulations. All simulations were performed with the recently implemented GPU-TI modules<sup>14,17</sup> built against the CUDA 10.1 GPU library and run on various GPU workstations and servers equipped with NVIDIA GTX 1080TI, RTX 2080 TI, Titan V, and V100 GPUs. Results reported were created with the single precision calculation/flexible precision accumulation (SPFP) model.<sup>72</sup>

The setups and protocols for AMBER standard GPU-accelerated TI simulations<sup>14,17</sup> are employed. The AMBER ff14SB force field<sup>73</sup> is used for standard amino acids, and GAFF<sup>74</sup> with the the AM1-BCC charges<sup>75,76</sup> for molecules without AMBER parameters. The TIP3P water model<sup>77</sup> is utilized. The `parmed` module of AMBER18 was used to prepare the topology files for TI calculations. The SHAKE algorithm<sup>78,79</sup> is used to constrain bonds between heavy atoms and hydrogens, except in the mutating parts, where no SHAKE is applied. Long-range electrostatic interactions were treated by the particle-mesh Ewald method (PME).<sup>70</sup> A cut-off of 10 Å for the model systems (see below sections) and the hydration free energy calculations, and 8 Å for RBFEs, is used for non-bonded interactions, including the direct space terms of the PME method and particles interacting through softcore potentials. The Ewald error tolerance is set to  $10^{-5}$  and the Ewald coefficient is automatically set according to the error tolerance and non-bonded cut-off. The model systems are simulated with the NVT ensemble at 300K while the hydration free energy and the RBEF simulations are performed with the NPT ensemble regulated at 1.0 atm at 298K. Detailed setups and protocols for individual systems can be found in the Supporting Information.

## Results

Here we develop a  $P$ -order smoothstep softcore potential,  $\text{SSC}(P)$ , to overcome problems inherent in concerted transformations with the conventional softcore potential<sup>36</sup> currently used in many molecular simulation packages. While many values of  $P$  have been explored in this work,  $P=2$  (second order) was found to have the most reliable performance and hence will be the focus in the following results and discussion. Nevertheless, higher orders of  $P$  may be useful for specific scenarios not encountered in this work and therefore this variable has been retained for the user to adjust, with  $P=2$  being the default in AMBER20. We begin by examining a select set of alchemical transformations in solution that represent edge cases that help to illustrate the origin of the endpoint catastrophe, particle collapse and large gradient-jump problems, and how these problems can be overcome by use of the  $\text{SSC}(2)$  with optimized parameters. We first demonstrate below how  $\text{SSC}(2)$  can robustly handle concerted alchemical transformations for a variety of absolute and relative hydration free energies of molecules in comparison with benchmark stepwise (decharge-vdW-recharge) transformations. Next we consider a more complex set of alchemical transformations involving protein-ligand binding that represent edge cases where the conventional softcore potential fails (sometimes dramatically) for concerted transformations, and demonstrate that the  $\text{SSC}(2)$  potential overcomes these problems. We then demonstrate that the  $\text{SSC}(2)$  potential can reproduce benchmark stepwise transformations for a broad range of RBFs, including ligand sets for six additional protein targets.

### Illustration of problems using original AMBER softcore potentials and proposed solutions

In this section, we examine a set of simple edge cases that illustrate the endpoint catastrophe, particle collapse and large gradient-jump problems, and go on to propose a solution using a new second-order smoothstep softcore potential,  $\text{SSC}(2)$ , with optimized parameters. The

1  
2  
3 test cases involving absolute and relative hydration free energies (gas phase part of the cycle  
4 is not considered in these illustrations) are as follows. The first test case involves calculation  
5 of the absolute hydration free energy of 3,4-diphenyltoluene (denoted as the DPT/0), a bulky  
6 fairly hydrophobic system, which will be made to vanish in solution. The second test case  
7 is the absolute hydration free energy of a  $\text{Na}^+$  ion (denoted  $\text{Na}^+/0$ ), a small charged system  
8 that will introduce new issues when made to vanish in solution. The third test system is the  
9 relative hydration free energy of two Factor Xa ligands,<sup>14,80</sup> L51c and L51h, involving the  
10 transformation  $\text{L51c} \rightarrow \text{L51h}$  in solution (denoted as L51c/h), involving migration of charge  
11 from one region of the ligand to another.  
12  
13  
14  
15  
16  
17  
18  
19  
20  
21

### 22 **Results of the original AMBER softcore potentials:**

23  
24  
25 Figure 1 shows the  $\langle dU/d\lambda \rangle_\lambda$  vs.  $\lambda$  plots for alchemical free energy simulations of these test  
26 systems using the one-step concerted scheme and different  $\alpha$  and  $\beta$  softcore parameters. The  
27 DPT/0 (upper panels), L51c/h (middle panels) and  $\text{Na}^+/0$  (lower panels) transformations  
28 are shown in solution. The original AMBER softcore potential form of Equation (4) is used,  
29 or equivalently the zeroth order smoothstep softcore function,  $\text{SSC}(0)$ , of Equation (23),  
30 in the results shown in the first three left columns while the results from the proposed  
31 smoothstep softcore potential  $\text{SSC}(2)$  are shown in the rightmost column.  
32  
33  
34  
35  
36  
37  
38

39 Consider first the leftmost panels in Figure 1, corresponding to a  $\beta$  value of  $12 \text{ \AA}^2$ , which  
40 is the default value in AMBER18. For this value of  $\beta$ , with small  $\alpha$  values (0.05 and 0.2),  
41 the endpoint “catastrophe” is formally averted, but its effects are still clearly prevalent for  
42 DPT/0 (large negative  $\langle dU/d\lambda \rangle_\lambda$  at  $\lambda=1$ ) and L51c/h (large positive  $\langle dU/d\lambda \rangle_\lambda$  at  $\lambda=0$  and  
43 large negative at  $\lambda=1$ ), whereas it is much less apparent for  $\text{Na}^+/0$  which involves much  
44 smaller steric annihilation.  
45  
46  
47  
48  
49  
50

51 Softening the repulsive potential by using a larger value of  $\alpha$  (0.5), reduces the problems  
52 at the endpoints, but leads to other issues at intermediate states. Specifically, for L51c/h  
53 the profiles are not smooth for  $\lambda$  values between 0.2 and 0.4, and  $\lambda \sim 0.8$ , and for  $\text{Na}^+/0$  for  
54  
55  
56  
57  
58  
59  
60

1  
2  
3  $\lambda \sim 0.2$ . The origin of this irregularity is the particle collapse problem, where at some inter-  
4 mediate  $\lambda$  values, the softened exchange repulsions (large  $\alpha$ ) can no longer counterbalance  
5 the attractive softcore Coulomb attractions of oppositely charged particles, causing them to  
6 collapse on top of one another, and leading to sampling issues.  
7  
8

9  
10  
11 This imbalance can be reduced by increasing the value of  $\beta$ , as is indicated by the second  
12 leftmost ( $\beta=17 \text{ \AA}^2$ ) and third leftmost ( $\beta=50 \text{ \AA}^2$ ) columns of panels in Figure 1, which  
13 softens the electrostatic interactions. With  $\beta$  set to  $17 \text{ \AA}^2$ , the  $\langle dU/d\lambda \rangle_\lambda$  curve for L51c/h is  
14 much improved relative to  $\beta=12 \text{ \AA}^2$ , particularly for the  $\alpha$  values of 0.05 and 0.2. In the case  
15 of  $\text{Na}^+/0$ , the strong electrostatic interactions require a  $\beta$  value of  $50 \text{ \AA}^2$  to achieve stable  
16 (smooth)  $\langle dU/d\lambda \rangle_\lambda$  curves for  $\alpha$  values of 0.05 and 0.2.  
17  
18

19  
20  
21 However, the large value of  $\beta$  required to address the particle collapse problem also has the  
22 effect of leading to much larger values of  $\langle dU/d\lambda \rangle_\lambda$  that arise from the derivative (gradient)  
23 term in Equation (19) that is scaled by  $\beta$ . In the  $\text{Na}^+/0$  transformation, this manifests as  
24 a dramatic rise in  $\langle dU/d\lambda \rangle_\lambda$  at  $\lambda=0$  for larger  $\beta$  values. This is the large gradient-jump  
25 problem, which has also been discussed by others.<sup>37</sup>  
26  
27

28  
29  
30 At this point, we conclude that the default softcore potential parameters  $\alpha/\beta$  in AM-  
31 BER18,  $0.5/12 \text{ \AA}^2$ , are useful to adequately address the “endpoint catastrophe” for the edge  
32 cases considered here, but have considerable susceptibility to the “particle collapse” problem.  
33 The particle collapse problem can be addressed by reducing  $\alpha$  to harden the short-ranged re-  
34 pulsions of the softcore LJ potential, and increasing  $\beta$  to soften the electrostatic interactions.  
35 Nonetheless, with this strategy for choice of  $\alpha$  and  $\beta$ , using the conventional linear softcore  
36 scheme of Equation (4), it does not appear possible to simultaneously address the endpoint  
37 catastrophe, particle collapse, and large gradient-jump problems, arising from small values  
38 of  $\alpha$  and large values of  $\beta$ , respectively.  
39  
40  
41  
42  
43  
44  
45  
46  
47  
48  
49  
50  
51  
52  
53  
54  
55  
56  
57  
58  
59  
60

## Development of a second-order smoothstep softcore potential

We now consider an alternative smoothstep softcore function, which employs a second-order smoothstep function, SSC(2), as described in Equation (23). The rightmost column of Figure 1 shows the  $\langle dU/d\lambda \rangle_\lambda$  vs.  $\lambda$  plots for alchemical free energy simulations of the same systems as Figure 1, but with the SSC(2) softcore potential as opposed to the original AMBER softcore potential. To be clear, only results with re-optimized softcore parameters ( $\alpha=0.2$ ,  $\beta=50 \text{ \AA}^2$ ) are shown here. The results using the SSC(2) potential with other combinations of  $\alpha/\beta$  can be found in Figure S2 of Supporting Information.

The first thing that is clearly apparent is that the behavior at all of the  $\lambda=0$  and 1 endpoints have greatly improved. This is because the derivatives of the smoothstep function vanish at the endpoints, making the first term in brackets in Equation (24) also go to zero at  $\lambda=0$  and 1. In fact, it is clear from Equation (24) that the conventional thermodynamic derivative of the softcore potential is multiplied by a term that involves the derivative of the smoothstep function, which is zero at the endpoints for all orders greater than zero (in which case the derivative is unity). This also has the consequence that the “large gradient-jump” problem due to large values of  $\beta$  at the endpoints is also no longer an issue.

The use of the smoothstep function alone theoretically does not resolve the particle collapse problem. Rather, it allows stable adjustment of the  $\alpha/\beta$  softcore parameters to overcome the particle collapse, without the adverse consequences of the endpoint and large gradient-jump problems that occur when the conventional softcore potential is used. Note that, from Equation (25), the total softcore contributions to  $\langle dU/d\lambda \rangle_\lambda$  will be exactly zero at the end points, but the  $\langle dU/d\lambda \rangle_\lambda$  results shown in Figure 1 are not zero because of other interactions terms, which currently are not treated with the proposed SSC scheme.

For  $\alpha/\beta$  values of  $0.2/50 \text{ \AA}^2$ , all of the edge cases examined here appear quite stable. Higher order smoothstep functions approach the endpoints more gradually and smoothly, at a consequence of having a steeper slope in the transition between 0 and 1 in the intermediate  $\lambda$  values (Figure S1 of Supporting Information). Comparison of smoothstep functions of

1  
2  
3 different orders indicated a good balance between these properties was to use a second-order  
4 smoothstep function (see Supporting Information for details). In the remainder of the paper,  
5 we will use the SSC(2) potential together with  $\alpha/\beta$  values of 0.2/50 Å<sup>2</sup> to test and validate  
6 against a broad range of hydration free energy and RBF E calculations.  
7  
8  
9

## 10 11 12 13 **Hydration free energies of small organic molecules** 14

15 Here we examine absolute and relative hydration free energies of a series of small organic  
16 molecules that have been recently employed to verify the reproducibility of free energy cal-  
17 culations across different molecular simulation software packages.<sup>81</sup> The purpose is to verify  
18 that the SSC(2) potential, with parameters adjusted by consideration of the edge cases in  
19 the previous section, is robust in reproducing results from the stepwise scheme. Table 1 lists  
20 the free energy values for alchemical transformations representing the absolute (de)hydration  
21 free energies for 9 organic molecules as well as several relative hydration free energies. Results  
22 from simulations of concerted transformations with the original AMBER softcore potential  
23 and 2nd-order smoothstep softcore potential, SSC(2), are compared with reference calcu-  
24 lations using the stepwise approach with original AMBER softcore potential and BAR<sup>65</sup>  
25 analysis. In most cases, the differences between the free energy values with respect to the  
26 reference results, designated as  $\Delta$  in the table, are comparable to or less than the error esti-  
27 mates of the results themselves. A minor exception occurs for the absolute dehydration free  
28 energy of methanol (3.78 kcal/mol) which is slightly overestimated with both the original  
29 AMBER softcore potential and SSC(2) by 0.06-0.07 kcal/mol. The largest deviation with  
30 respect to the reference values occurs for the methanol  $\rightarrow$  ethane transformation which is  
31 overestimated by 0.68 kcal/mol with the original AMBER softcore potential, whereas SSC(2)  
32 agrees closely (0.02 kcal/mol). The only instance where SSC(2) performs statistically more  
33 poorly than the original AMBER softcore potential is for the 7-CPI  $\rightarrow$  2-CPI transformation,  
34 which is overestimated by 0.15 kcal/mol with SSC(2) whereas the original AMBER softcore  
35 potential is closer to the reference result (0.04 kcal/mol). Overall, the error estimates for  
36  
37  
38  
39  
40  
41  
42  
43  
44  
45  
46  
47  
48  
49  
50  
51  
52  
53  
54  
55  
56  
57  
58  
59  
60



1  
2  
3 SSC(2) appear very slightly larger than the original AMBER softcore potential, and overall  
4 the results are quite comparable, except in the instances of the edge cases where SSC(2)  
5 provides accurate results whereas the original AMBER softcore potential fails.  
6  
7  
8  
9

## 10 **RBFE calculation of 8 published protein systems**

11  
12  
13 In this section we examine more complex cases of RBFE on a series of previously studied  
14 drug targets.<sup>82</sup> This set (defined as the JACS set) covers eight protein systems and 200  
15 ligand mutations and has been widely used as a benchmark test set for tractable RBFE  
16 calculations without significant conformational changes or other challenging scenarios such  
17 as changes in tautomer/ionization states or buried waters. We first examine two systems  
18 that demonstrate significant edge cases where the original AMBER softcore potential fails,  
19 whereas the SSC(2) potential is shown to be accurate. Next we examine the six additional  
20 protein-ligand systems to demonstrate the SSC(2) is also robust.  
21  
22  
23  
24  
25  
26  
27  
28  
29  
30

### 31 **Results of the two problematic protein targets: PTP1B and p38**

32  
33 Out of the JACS set, two protein targets (PTP1B and p38) demonstrated significant edge  
34 cases where the conventional softcore potential with default parameters was observed to fail.  
35 The RBFE predictions for PTP1B ligands are plotted in Figure 2, comparing the stepwise  
36 scheme (x-axis) and the concerted scheme (y-axis). The upper two panels show the results for  
37 the original softcore potential parameter set analyzed by TI (left panels) and MBAR (right  
38 panels). The lower two panels show the corresponding results for the SSC(2) smoothstep  
39 softcore potential. It is clear that the original AMBER softcore potential produces several  
40 prominent outlier points with respect to the stepwise scheme. These outliers are exacerbated  
41 for the TI results, which are more sensitive to the integration of thermodynamic derivatives.  
42 Nonetheless, the MBAR results are clearly problematic with the original softcore potential.  
43 With the use of the SSC(2) smoothstep softcore potential, the RBFE results agree with those  
44 of the stepwise scheme to within statistical error estimates, and the TI and MBAR results  
45  
46  
47  
48  
49  
50  
51  
52  
53  
54  
55  
56  
57  
58  
59  
60

1  
2  
3 are virtually identical.  
4

5 Analogous results for p38 ligands are plotted in Figure 3. Again, with the original AM-  
6 BER softcore potential, both TI and MBAR produce several outlier points that vary dra-  
7 matically from the reference results computed with the stepwise scheme. With the SSC(2)  
8 smoothstep softcore potential, results are in close agreement (within statistical error esti-  
9 mates, typically less than 1 kcal/mol) of the reference values. Further, the TI and MBAR  
10 results are almost indistinguishable. Hence, it appears that the SSC(2) smoothstep softcore  
11 potential can successfully overcome limitations of the original AMBER softcore potential for  
12 the problematic edge cases considered here.  
13  
14  
15  
16  
17  
18  
19  
20  
21

## 22 **Results of the six well-behaved protein targets:**

23  
24  
25 The RBFE results for the renaming 6 targets of the JACS data set using the concerted  
26 scheme are shown in Figure 4 for the original AMBER softcore scheme and the Figure 5  
27 proposed SSC(2) scheme, respectively. Plots show the comparison between the stepwise  
28 scheme (x-axis) and the reported concerted scheme (y-axis). The dashed red lines indicate  
29 the region of  $\pm 1.0$  kcal/mol difference. The corresponding standard deviations are plotted  
30 as gray error bars and also shown in the small blue plots.  
31  
32  
33  
34  
35  
36

37 The original AMBER softcore scheme results (Figure 4) for these six targets indicate  
38 that the concerted scheme produces virtually the same RBFE (within 1.0 kcal/mol) results  
39 compared to the stepwise scheme, except one outlier in the Jnk1 case. The standard devia-  
40 tions from the concerted and the stepwise schemes are also roughly similar and correlated.  
41 The proposed SSC(2) scheme results (Figure 5) are qualitatively similar, except the single  
42 Jnk1 outlier now disappears. Nevertheless, compared the correlation coefficients ( $R^2$ ), the  
43 proposed SSC(2) scheme delivers better results for MCL1 (0.80 vs. 0.99) and Jnk1 (0.92 vs.  
44 0.99). Hence for these six targets, the proposed SSC(2) scheme at least performs as well as  
45 the original AMBER softcore approach and they produces virtually the same RBFE (within  
46 1.0 kcal/mol) results compared to the stepwise scheme, except few points near or on the  
47  
48  
49  
50  
51  
52  
53  
54  
55  
56  
57  
58  
59  
60

1  
2  
3 1.0 kcal/mol error lines, which all have large errors in both the concerted and the stepwise  
4 schemes. This might imply that other hidden issues besides the softcore potentials need to  
5 be further investigated.  
6  
7  
8  
9

## 11 Discussion

12  
13  
14 Although it is one of the most pivotal decisions in setting up a free energy simulations, the  
15 choice of alchemical pathway essentially remains an unsolved issue. For many transforma-  
16 tions, existing softcore potential implementations are stable and lead to numerically satis-  
17 factory results. However, many seemingly benign transformations can sporadically and/or  
18 unexpectedly become unstable with no obvious indication as to the underlying issue. To be  
19 clear, this is a separate problem from the standard simulation issues of adequate statistical  
20 sampling and accurate force field modeling. Indeed, the issue is considerably more funda-  
21 mental since a numerically unstable algorithm can neither sample exhaustively nor correctly  
22 characterize even a “perfect” physical model. The previous sections showed several examples  
23 where these failures occur using the standard softcore implementation in AMBER. Although  
24 we do not present specific evidence here, we feel that the data provides a reasonable indi-  
25 cation that other related implementations would likely lead to similar failures on at least  
26 some of these examples. Regardless, the SSC(2) potential resolves the issues in nearly all  
27 instances, except when overall certainty is precluded by a system that is challenging for other  
28 reasons (e.g. slow degrees of freedom or high variability). Even so, this is still an absence of  
29 evidence that SSC(2) fails and not evidence that SSC(2) does not fail – there may indeed be  
30 situations where the issues outlined here are not resolved by SSC(2). Hence, as a community  
31 it is important to continue to build up benchmark datasets and to document their known  
32 pathologies.  
33  
34  
35  
36  
37  
38  
39  
40  
41  
42  
43  
44  
45  
46  
47  
48  
49  
50  
51

52 Other authors have also considered alchemical path selection in detail. Most notably,  
53 this has been done in the context of non-equilibrium schemes where the path implies a time-  
54  
55  
56  
57  
58  
59  
60

1  
2  
3 dependent protocol.<sup>83,84</sup> Indeed, there has recently been revived interest in this approach  
4 for ligand binding calculations due to its focus on explicit bound/unbound states.<sup>85</sup> How-  
5 ever, this technique is not considered here and it is not obvious that the developments here  
6 would transfer. This is because the success of non-equilibrium methods seem to be more  
7 strongly conditioned on fluctuations at the endpoints, both in terms of their magnitude and  
8 timescale.<sup>86</sup> While this is essentially the same as the endpoint catastrophe, the current ap-  
9 proach is also concerned with discontinuities *along* the path, as these are more central in  
10 TI. Shirts and co-workers have considered the problem of finding a minimum variance path  
11 in equilibrium alchemical schemes and found that the fluctuations at intermediate states  
12 (especially the timescales thereof) are of critical importance.<sup>40,41</sup> Recently, Pai and Gallic-  
13 chio proposed a capped form of softcore potential and offer a general design strategy of the  
14 alchemical pathways.<sup>38</sup>

15  
16  
17  
18  
19  
20  
21  
22  
23  
24  
25  
26  
27  
28  
29  
30  
31  
32  
33  
34  
35  
36  
37  
38  
39  
40  
41  
42  
43  
44  
45  
46  
47  
48  
49  
50  
51  
52  
53  
54  
55  
56  
57  
58  
59  
60

The stepwise scheme has been widely thought to be the most stable procedure for per-  
forming TI calculations. Employing the smoothstep softcore potential, TI calculations can  
be performed in a single concerted transformation without a loss of precision compared to  
the stepwise scheme. Consequently, the single concerted transformation with the smooth-  
step potential should be preferred as it requires much less setup steps and computational  
resources.

The calculations shown in this paper mainly utilized the thermodynamic integration  
method. Nonetheless, our data suggests that many of the pathological problems discussed  
in the context of TI are also problematic for other free energy approaches such as ther-  
modynamic perturbation<sup>56</sup> with BAR<sup>65</sup> or MBAR<sup>69</sup> analysis. Our results of PTP1B and  
p38 (Figures 2 and 3) demonstrate that the SSC(2) potential also eliminates the observed  
problems that occur with thermodynamic perturbation methods with MBAR analysis, and  
converge to the same result as TI.

Furthermore, the proposed SSC(2) scheme is well suited for advanced  $\lambda$ -scheduling op-  
timization and enhanced sampling schemes in the  $\lambda$ -space where a single-pass concerted  $\lambda$

1  
2  
3 transformation is desirable, including  $\lambda$  dynamics,<sup>43–46</sup> Hamiltonian replica exchange meth-  
4 ods,<sup>47–51</sup> adaptive biasing<sup>44,52,53</sup> or self-adjusted mixture sampling<sup>54,55</sup> methods. We are  
5 actively investigating possible incorporation of the proposed SSC(2) potential with these  
6 techniques.  
7  
8  
9

## 10 11 12 13 Conclusion

14  
15  
16 In conclusion, we propose a novel second-order smoothstep softcore potential, SSC(2), to  
17 overcome the endpoint catastrophe, particle collapse, and large gradient-jump problems rou-  
18 tinely encountered in alchemical free energy simulations using concerted transformations.  
19 These problems stem from poor phase space overlap, imbalance of Coulomb attraction and  
20 exchange-repulsion, and thermodynamic derivative terms in the softcore potential that lead  
21 to sensitivity to softcore  $\alpha$  and particularly  $\beta$  parameters. The SSC(2) smoothstep softcore  
22 potential with  $\alpha=0.2$  and  $\beta=50 \text{ \AA}^2$  has been demonstrated to overcome these problems for a  
23 broad set of alchemical transformations used in the calculation of hydration free energies and  
24 RBFEs. The key characteristic of the smoothstep softcore function is that the weights used in  
25 the alchemical transformation have derivatives that vanish at the transformation endpoints  
26 ( $\lambda=0$  and  $1$ ), and enable smooth adjustment of the  $\lambda$ -dependent terms in the potential. This  
27 in turn allows Coulomb attraction and exchange-repulsions to be rebalanced so as to avoid  
28 introduction of artificial minima where a particle in the softcore region can collapse on a  
29 neighboring particle at intermediate  $\lambda$  states. Results are examined for edge cases where the  
30 original AMBER softcore potential is observed to fail, and the SSC(2) smoothstep softcore  
31 potential is shown to remain accurate. The SSC(2) potential is further tested against a  
32 broad set of hydration free energy and RBFEs for the JACS dataset containing 200 ligands  
33 and spanning 8 protein targets. The SSC(2) potential developed here is demonstrated to  
34 be highly robust, leading to precise free energy values for all the systems considered here.  
35 The SSC(2) potential has the advantage that it can be used in concerted transformations  
36  
37  
38  
39  
40  
41  
42  
43  
44  
45  
46  
47  
48  
49  
50  
51  
52  
53  
54  
55  
56  
57  
58  
59  
60

1  
2  
3 with less computational effort than the stepwise scheme, and is better suited for enhanced  
4 sampling methods with more advanced, adaptive  $\lambda$  scheduling requirements.  
5  
6  
7

## 8 9 **Acknowledgement**

10  
11  
12 The authors are grateful for financial support provided by the National Institutes of Health  
13 (No. GM107485 to DMY). Computational resources were provided by the Office of Advanced  
14 Research Computing (OARC) at Rutgers, The State University of New Jersey, the National  
15 Institutes of Health under Grant No. S10OD012346, the Blue Waters sustained-petascale  
16 computing project (NSF OCI 07-25070, PRAC OCI-1515572), and by the Extreme Science  
17 and Engineering Discovery Environment (XSEDE), which is supported by National Science  
18 Foundation grant number No. ACI-1548562.<sup>87</sup> This work used the XSEDE resource COMET  
19 and COMET GPU at SDSC through allocation TG-CHE190067. We gratefully acknowledge  
20 the support of the NVIDIA Corporation with the donation of several Pascal, Volta, and  
21 Turing GPUs and the GPU-time of a GPU-cluster where the reported benchmark results  
22 were performed.  
23  
24  
25  
26  
27  
28  
29  
30  
31  
32  
33  
34  
35  
36

## 37 **References**

- 38  
39  
40 (1) Stone, J. E.; Phillips, J. C.; Freddolino, P. L.; Hardy, D. J.; Trabuco, L. G.; Schul-  
41 ten, K. Accelerating molecular modeling applications with graphics processors. *J. Com-*  
42 *put. Chem.* **2007**, *28*, 2618–2640.  
43  
44  
45  
46 (2) Anderson, J. A.; Lorenz, C. D.; Travesset, A. General purpose molecular dynamics  
47 simulations fully implemented on graphics processing units. *J. Comput. Phys.* **2008**,  
48 *227*, 5342–5359.  
49  
50  
51  
52  
53 (3) Hardy, D. J.; Stone, J. E.; Schulten, K. Multilevel Summation of Electrostatic Potentials  
54 Using Graphics Processing Units. *Parallel Computing* **2009**, *35*, 164–177.  
55  
56  
57  
58  
59  
60

- 1  
2  
3 (4) Harvey, M. J.; Giupponi, G.; Fabritiis, G. D. ACEMD: Accelerating Biomolecular Dy-  
4 namics in the Microsecond Time Scale. *J. Chem. Theory Comput.* **2009**, *5*, 1632–1639.  
5  
6  
7  
8 (5) Harvey, M. J.; De Fabritiis, G. An Implementation of the Smooth Particle Mesh Ewald  
9 Method on GPU Hardware. *J. Chem. Theory Comput.* **2009**, *5*, 2371–2377.  
10  
11  
12 (6) Stone, J. E.; Hardy, D. J.; Ufimtsev, I. S.; Schulten, K. GPU-accelerated molecular  
13 modeling coming of age. *J. Mol. Graphics Model.* **2010**, *29*, 116–125.  
14  
15  
16 (7) Farber, R. M. Topical perspective on massive threading and parallelism. *J. Mol. Graph-*  
17 *ics Model.* **2011**, *30*, 82–89.  
18  
19  
20 (8) Göetz, A.; Williamson, M. J.; Xu, D.; Poole, D.; Le Grand, S.; Walker, R. C. Routine  
21 microsecond molecular dynamics simulations with AMBER on GPUs. 1. Generalized  
22 Born. *J. Chem. Theory Comput.* **2012**, *8*, 1542.  
23  
24  
25 (9) Eastman, P. et al. OpenMM 4: A Reusable, Extensible, Hardware Independent Library  
26 for High Performance Molecular Simulation. *J. Chem. Theory Comput.* **2013**, *9*, 461–  
27 469.  
28  
29  
30 (10) Salomon-Ferrer, R.; Götz, A. W.; Poole, D.; Le Grand, S.; Walker, R. C. Routine mi-  
31 crosecond molecular dynamics simulations with AMBER on GPUs. 2. Explicit solvent  
32 Particle Mesh Ewald. *J. Chem. Theory Comput.* **2013**, *9*, 3878–3888.  
33  
34  
35 (11) Chipot, C. Frontiers in free-energy calculations of biological systems. *WIREs Comput.*  
36 *Mol. Sci.* **2014**, *4*, 71–89.  
37  
38  
39 (12) Eastman, P.; Swails, J.; Chodera, J. D.; McGibbon, R. T.; Zhao, Y.; Beauchamp, K. A.;  
40 Wang, L.-P.; Simmonett, A. C.; Harrigan, M. P.; Stern, C. D.; Wiewiora, R. P.;  
41 Brooks, B. R.; Pande, V. S. OpenMM 7: Rapid development of high performance  
42 algorithms for molecular dynamics. *PLoS Comput. Biol.* **2017**, *13*, 1005659–1005659.  
43  
44  
45  
46  
47  
48  
49  
50  
51  
52  
53  
54  
55  
56  
57  
58  
59  
60

- 1  
2  
3 (13) Abel, R.; Wang, L.; Harder, E. D.; Berne, B. J.; Friesner, R. A. Advancing Drug  
4 Discovery through Enhanced Free Energy Calculations. *Acc. Chem. Res.* **2017**, *50*,  
5 1625–1632.  
6  
7  
8  
9  
10 (14) Lee, T.-S.; Hu, Y.; Sherborne, B.; Guo, Z.; York, D. M. Toward Fast and Accurate  
11 Binding Affinity Prediction with pmemdGTI: An Efficient Implementation of GPU-  
12 Accelerated Thermodynamic Integration. *J. Chem. Theory Comput.* **2017**, *13*, 3077–  
13 3084.  
14  
15  
16  
17  
18 (15) Mermelstein, D. J.; Lin, C.; Nelson, G.; Kretsch, R.; McCammon, J. A.; Walker, R. C.  
19 Fast and flexible gpu accelerated binding free energy calculations within the amber  
20 molecular dynamics package. *J. Comput. Chem.* **2018**, *39*, 1354–1358.  
21  
22  
23  
24  
25 (16) Giese, T. J.; York, D. M. A GPU-Accelerated Parameter Interpolation Thermodynamic  
26 Integration Free Energy Method. *J. Chem. Theory Comput.* **2018**, *14*, 1564–1582.  
27  
28  
29  
30 (17) Lee, T.-S.; Cerutti, D. S.; Mermelstein, D.; Lin, C.; LeGrand, S.; Giese, T. J.; Roit-  
31 berg, A.; Case, D. A.; Walker, R. C.; York, D. M. GPU-Accelerated Molecular Dynamics  
32 and Free Energy Methods in Amber18: Performance Enhancements and New Features.  
33 *J. Chem. Inf. Model.* **2018**, *58*, 2043–2050.  
34  
35  
36  
37  
38 (18) Song, L. F.; Lee, T.-S.; Zhu, C.; York, D. M.; Merz Jr., K. M. Using AMBER18 for  
39 Relative Free Energy Calculations. *J. Chem. Inf. Model.* **2019**, *59*, 3128–3135.  
40  
41  
42  
43 (19) Chipot, C., Pohorille, A., Eds. *Free Energy Calculations: Theory and Applications in*  
44 *Chemistry and Biology*; Springer Series in Chemical Physics; Springer: New York, 2007;  
45 Vol. 86.  
46  
47  
48  
49  
50 (20) Chodera, J.; Mobley, D.; Shirts, M.; Dixon, R.; Branson, K.; Pande, V. Alchemical free  
51 energy methods for drug discovery: progress and challenges. *Curr. Opin. Struct. Biol.*  
52 **2011**, *21*, 150–160.  
53  
54  
55  
56  
57  
58  
59  
60



- 1  
2  
3 (21) Christ, C.; Mark, A.; van Gunsteren, W. Basic Ingredients of Free Energy Calculations:  
4 A Review. *J. Comput. Chem.* **2010**, *31*, 1569–1582.  
5  
6  
7  
8 (22) Foloppe, N.; Hubbard, R. Towards Predictive Ligand Design With Free-Energy Based  
9 Computational Methods? *Curr. Med. Chem.* **2006**, *13*, 3583–3608.  
10  
11  
12 (23) Pohorille, A.; Jarzynski, C.; Chipot, C. Good Practices in Free-Energy Calculations. *J.*  
13 *Phys. Chem. B* **2010**, *114*, 10235–10253.  
14  
15  
16 (24) Gallicchio, E.; Levy, R. M. Advances in all atom sampling methods for modeling  
17 protein-ligand binding affinities. *Curr. Opin. Struct. Biol.* **2011**, *21*, 161–166.  
18  
19  
20 (25) Hansen, N.; van Gunsteren, W. F. Practical Aspects of Free-Energy Calculations: A  
21 Review. *J. Chem. Theory Comput.* **2014**, *10*, 2632–2647.  
22  
23  
24 (26) Jorgensen, W. L. Efficient drug lead discovery and optimization. *Acc. Chem. Res.* **2009**,  
25 *42*, 724–733.  
26  
27  
28 (27) Michel, J.; Essex, J. W. Prediction of protein-ligand binding affinity by free energy  
29 simulations: assumptions, pitfalls and expectations. *J. Comput.-Aided Mol. Des.* **2010**,  
30 *24*, 639–658.  
31  
32  
33 (28) Mobley, D. L.; Dill, K. A. Binding of Small-Molecule Ligands to Proteins: What You  
34 See Is Not Always What You Get. *Structure* **2009**, *17*, 489–498, 0969-2126.  
35  
36  
37 (29) Mobley, D. L.; Klimovich, P. V. Perspective: Alchemical free energy calculations for  
38 drug discovery. *J. Chem. Phys.* **2012**, *137*, 230901.  
39  
40  
41 (30) Gumbart, J. C.; Roux, B.; Chipot, C. Standard Binding Free Energies from Computer  
42 Simulations: What Is the Best Strategy? *J. Chem. Theory Comput.* **2013**, *9*, 794–802.  
43  
44  
45 (31) Mezei, M. Polynomial path for the calculation of liquid state free energies from computer  
46 simulations tested on liquid water. *J. Comput. Chem.* **1992**, *13*, 651–656.  
47  
48  
49  
50  
51  
52  
53  
54  
55  
56  
57  
58  
59  
60

- 1  
2  
3 (32) Resat, H.; Mezei, M. Studies on free energy calculations. I. Thermodynamic integration  
4 using a polynomial path. *J. Chem. Phys.* **1993**, *99*, 6052–6061.  
5  
6  
7  
8 (33) Simonson, T. Free energy of particle insertion. *Mol. Phys.* **1993**, *80*, 441–447.  
9  
10  
11 (34) Beutler, T. C.; Mark, A. E.; René C. van Schaik and Paul R. Gerber and Wilfred F. van  
12 Gunsteren, Avoiding singularities and numerical instabilities in free energy calculations  
13 based on molecular simulations. *Chem. Phys. Lett.* **1994**, *222*, 529–539.  
14  
15  
16  
17 (35) Steinbrecher, T.; Mobley, D. L.; Case, D. A. Nonlinear scaling schemes for Lennard-  
18 Jones interactions in free energy calculations. *J. Chem. Phys.* **2007**, *127*, 214108.  
19  
20  
21  
22 (36) Steinbrecher, T.; Joung, I.; Case, D. A. Soft-Core Potentials in Thermodynamic In-  
23 tegration: Comparing One- and Two-Step Transformations. *J. Comput. Chem.* **2011**,  
24 *32*, 3253–3263.  
25  
26  
27  
28  
29 (37) Gapsys, V.; Seeliger, D.; de Groot, B. L. New Soft-Core Potential Function for Molec-  
30 ular Dynamics Based Alchemical Free Energy Calculations. *J. Chem. Theory Comput.*  
31 **2012**, *8*, 2373–2382.  
32  
33  
34  
35  
36 (38) Pal, R. K.; Gallicchio, E. Perturbation potentials to overcome order/disorder transitions  
37 in alchemical binding free energy calculations. *J. Chem. Phys.* **2019**, *151*, 124116.  
38  
39  
40  
41 (39) Jiang, W.; Chipot, C.; Roux, B. Computing Relative Binding Affinity of Ligands to Re-  
42 ceptor: An Effective Hybrid Single-Dual-Topology Free-Energy Perturbation Approach  
43 in NAMD. *J. Chem. Inf. Model.* **2019**, *59*, 3794–3802.  
44  
45  
46  
47  
48 (40) Pham, T. T.; Shirts, M. R. Identifying low variance pathways for free energy calculations  
49 of molecular transformations in solution phase. *J. Chem. Phys.* **2011**, *135*, 034114.  
50  
51  
52  
53 (41) Pham, T. T.; Shirts, M. R. Optimal pairwise and non-pairwise alchemical pathways for  
54 free energy calculations of molecular transformation in solution phase. *J. Chem. Phys.*  
55 **2012**, *136*, 124120.  
56  
57  
58

- 1  
2  
3 (42) Klimovich, P. V.; Shirts, M. R.; Mobley, D. L. Guidelines for the analysis of free energy  
4 calculations. *J. Comput.-Aided Mol. Des.* **2015**, *29*, 397–411.  
5  
6  
7  
8 (43) Ding, X.; Vilseck, J. Z.; Hayes, R. L.; Brooks, C. L. Gibbs Sampler-Based  $\lambda$ -Dynamics  
9 and Rao-Blackwell Estimator for Alchemical Free Energy Calculation. *J. Chem. Theory*  
10 *Comput.* **2017**, *13*, 2501–2510.  
11  
12  
13  
14 (44) Hayes, R. L.; Armacost, K. A.; Vilseck, J. Z.; Brooks, C. L. Adaptive Landscape  
15 Flattening Accelerates Sampling of Alchemical Space in Multisite  $\lambda$  Dynamics. *J. Phys.*  
16 *Chem. B* **2017**, *121*, 3626–3635.  
17  
18  
19  
20 (45) Guo, Z.; Brooks, C. L. Rapid Screening of Binding Affinities: Application of the  $\lambda$ -  
21 Dynamics Method to a Trypsin-Inhibitor System. *J. Am. Chem. Soc.* **1998**, *120*, 1920–  
22 1921.  
23  
24  
25  
26  
27 (46) Guo, Z.; Brooks, III, C. L.; Kong, X. Efficient and Flexible Algorithm for Free Energy  
28 Calculations Using the  $\lambda$ -Dynamics Approach. *J. Phys. Chem. B* **1998**, *102*, 2032–2036.  
29  
30  
31  
32 (47) Jiang, W.; Roux, B. Free energy perturbation Hamiltonian replica-exchange molecu-  
33 lar dynamics (FEP/H-REMD) for absolute ligand binding free energy calculations. *J.*  
34 *Chem. Theory Comput.* **2010**, *6*, 2559–2565.  
35  
36  
37  
38 (48) Arrar, M.; de Oliveira, C. A. F.; Fajer, M.; Sinko, W.; McCammon, J. A. w-REXAMD:  
39 A Hamiltonian replica exchange approach to improve free energy calculations for sys-  
40 tems with kinetically trapped conformations. *J. Chem. Theory Comput.* **2013**, *9*, 18–23.  
41  
42  
43  
44 (49) Itoh, S. G.; Okumura, H. Hamiltonian replica-permutation method and its applications  
45 to an alanine dipeptide and amyloid- $\beta$ (29-42) peptides. *J. Comput. Chem.* **2013**, *34*,  
46 2493–2497.  
47  
48  
49  
50  
51  
52 (50) Armacost, K. A.; Goh, G. B.; Brooks, C. L. Biasing Potential Replica Exchange Mul-  
53  
54  
55  
56  
57  
58  
59  
60

- 1  
2  
3        tisite  $\lambda$ -Dynamics for Efficient Free Energy Calculations. *J. Chem. Theory Comput.*  
4        **2015**, *11*, 1267–1277.  
5  
6  
7
- 8        (51) Yang, M.; Huang, J.; MacKerell, A. D. Enhanced Conformational Sampling Using  
9        Replica Exchange with Concurrent Solute Scaling and Hamiltonian Biasing Realized in  
10        One Dimension. *J. Chem. Theory Comput.* **2015**, *11*, 2855–2867.  
11  
12  
13
- 14        (52) Babin, V.; Roland, C.; Sagui, C. Adaptively biased molecular dynamics for free energy  
15        calculations. *J. Chem. Phys.* **2008**, *128*, 134101.  
16  
17  
18
- 19        (53) Darve, E.; Rodríguez-Gómez, D.; Pohorille, A. Adaptive biasing force method for scalar  
20        and vector free energy calculations. *J. Chem. Phys.* **2008**, *128*, 144120.  
21  
22  
23
- 24        (54) Carlson, D. E.; Stinson, P.; Pakman, A.; Paninski, L. *Proceedings of the 33rd Interna-*  
25        *tional Conference on Machine Learning; ICML'16; JMLR.org: New York, NY, USA,*  
26        *2016; Vol. 48; pp 2896–2905.*  
27  
28  
29
- 30  
31        (55) Tan, Z. Optimally Adjusted Mixture Sampling and Locally Weighted Histogram Anal-  
32        ysis. *J. Comput. Graph. Stat.* **2017**, *26*, 54–65.  
33  
34  
35
- 36        (56) Zwanzig, R. W. High-temperature equation of state by a perturbation method. I. Non-  
37        polar gases. *J. Chem. Phys.* **1954**, *22*, 1420–1426.  
38  
39  
40
- 41        (57) Kirkwood, J. G. Statistical mechanics of fluid mixtures. *J. Chem. Phys.* **1935**, *3*, 300–  
42        313.  
43  
44
- 45        (58) Straatsma, T. P.; Berendsen, H. J. Free energy of ionic hydration: Analysis of a thermo-  
46        dynamic integration technique to evaluate free energy differences by molecular dynamics  
47        simulations. *J. Chem. Phys.* **1988**, *89*, 5876–5886.  
48  
49  
50
- 51  
52        (59) Jarzynski, C. Nonequilibrium equality for free energy differences. *Phys. Rev. Lett.* **1997**,  
53        *78*, 2690–2693.  
54  
55  
56  
57  
58  
59  
60

- 1  
2  
3 (60) Crooks, G. E. Path-ensemble averages in systems driven far from equilibrium. *Phys.*  
4 *Rev. E* **2000**, *61*, 2361–2366.  
5  
6  
7  
8 (61) Boresch, S.; Woodcock, H. L. Convergence of single-step free energy perturbation. *Mol.*  
9 *Phys.* **2017**, *115*, 1200–1213.  
10  
11  
12 (62) Gapsys, V.; Michielssens, S.; Peters, J. H.; de Groot, B. L.; Leonov, H. Calculation of  
13 binding free energies. *Methods Mol. Biol.* **2015**, *1215*, 173–209.  
14  
15  
16  
17 (63) Jeong, D.; Andricioaei, I. Reconstructing equilibrium entropy and enthalpy profiles  
18 from non-equilibrium pulling. *J. Chem. Phys.* **2013**, *138*, 114110.  
19  
20  
21  
22 (64) Wei, D.; Song, Y.; Wang, F. A simple molecular mechanics potential for  $\mu\text{m}$  scale  
23 graphene simulations from the adaptive force matching method. *J. Chem. Phys.* **2011**,  
24 *134*, 184704.  
25  
26  
27  
28 (65) Bennett, C. H. Efficient estimation of free energy differences from Monte Carlo data.  
29 *J. Comput. Phys.* **1976**, *22*, 245–268.  
30  
31  
32  
33 (66) Torrie, G. M.; Valleau, J. P. Nonphysical sampling distributions in Monte Carlo free-  
34 energy estimation: Umbrella sampling. *J. Comput. Phys.* **1977**, *23*, 187–199.  
35  
36  
37  
38 (67) Lu, N.; Kofke, D. A. Accuracy of free-energy perturbation calculations in molecular  
39 simulation. I. Modeling. *J. Chem. Phys.* **2001**, *114*, 7303–7311.  
40  
41  
42  
43 (68) Shirts, M. R.; Pande, V. S. Comparison of efficiency and bias of free energies computed  
44 by exponential averaging, the Bennett acceptance ratio, and thermodynamic integra-  
45 tion. *J Chem Phys* **2005**, *122*, 144107.  
46  
47  
48  
49 (69) Shirts, M. R.; Chodera, J. D. Statistically optimal analysis of samples from multiple  
50 equilibrium states. *J. Chem. Phys.* **2008**, *129*, 124105.  
51  
52  
53  
54 (70) Darden, T.; York, D.; Pedersen, L. Particle mesh Ewald: An  $N \log(N)$  method for  
55 Ewald sums in large systems. *J. Chem. Phys.* **1993**, *98*, 10089–10092.  
56  
57  
58

- 1  
2  
3 (71) in't Veld, P. j.; Ismail, A. E.; Grest, G. S. Application of Ewald summations to long-  
4 range dispersion forces. *J. Chem. Phys.* **2007**, *127*, 144711.  
5  
6  
7  
8 (72) Le Grand, S.; Göetz, A. W.; Walker, R. C. SPFP: Speed without compromise—A mixed  
9 precision model for GPU accelerated molecular dynamics simulations. *Comput. Phys.*  
10 *Commun.* **2013**, *184*, 374–380.  
11  
12  
13  
14 (73) Maier, J. A.; Martinez, C.; Kasavajhala, K.; Wickstrom, L.; Hauser, K. E.; Simmer-  
15 ling, C. ff14SB: Improving the Accuracy of Protein Side Chain and Backbone Paramete-  
16 rters from ff99SB. *J. Chem. Theory Comput.* **2015**, *11*, 3696–3713.  
17  
18  
19  
20  
21 (74) Wang, J.; Wolf, R. M.; Caldwell, J. W.; Kollman, P. A.; Case, D. A. Development and  
22 testing of a general amber force field. *J. Comput. Chem.* **2004**, *25*, 1157–1174.  
23  
24  
25  
26 (75) Jakalian, A.; Jack, D. B.; Bayly, C. I. Fast, efficient generation of high-quality atomic  
27 charges. AM1-BCC model: II. parameterization and validation. *J. Comput. Chem.*  
28 **2002**, *23*, 1623–1641.  
29  
30  
31  
32  
33 (76) Jakalian, A.; Bush, B. L.; Jack, D. B.; Bayly, C. I. Fast, efficient generation of high-  
34 quality atomic charges. AM1-BCC model: I. method. *J. Comput. Chem.* **2000**, *21*,  
35 132–146.  
36  
37  
38  
39  
40 (77) Jorgensen, W. L.; Chandrasekhar, J.; Madura, J. D.; Impey, R. W.; Klein, M. L.  
41 Comparison of simple potential functions for simulating liquid water. *J. Chem. Phys.*  
42 **1983**, *79*, 926–935.  
43  
44  
45  
46  
47 (78) Ryckaert, J. P.; Ciccotti, G.; Berendsen, H. J. C. Numerical Integration of the Cartesian  
48 Equations of Motion of a System with Constraints: Molecular Dynamics of n-Alkanes.  
49 *J. Comput. Phys.* **1977**, *23*, 327–341.  
50  
51  
52  
53  
54 (79) Miyamoto, S.; Kollman, P. A. SETTLE: An analytic version of the SHAKE and RAT-  
55 TLE algorithms for rigid water models. *J. Comput. Chem.* **1992**, *13*, 952–962.  
56  
57  
58

- 1  
2  
3  
4  
5  
6  
7  
8  
9  
10  
11  
12  
13  
14  
15  
16  
17  
18  
19  
20  
21  
22  
23  
24  
25  
26  
27  
28  
29  
30  
31  
32  
33  
34  
35  
36  
37  
38  
39  
40  
41  
42  
43  
44  
45  
46  
47  
48  
49  
50  
51  
52  
53  
54  
55  
56  
57  
58  
59  
60
- (80) Lee, Y.-K.; Parks, D. J.; Lu, T.; Thieu, T. V.; Markotan, T.; Pan, W.; McComsey, D. F.; Milkiewicz, K. L.; Crysler, C. S.; Ninan, N.; Abad, M. C.; Giardino, E. C.; Maryanoff, B. E.; Damiano, B. P.; Player, M. R. 7-fluoroindazoles as potent and selective inhibitors of factor Xa. *J. Med. Chem.* **2008**, *51*, 282–297.
- (81) Loeffler, H. H.; Bosisio, S.; Duarte Ramos Matos, G.; Suh, D.; Roux, B.; Mobley, D. L.; Michel, J. Reproducibility of Free Energy Calculations across Different Molecular Simulation Software Packages. *J. Chem. Theory Comput.* **2018**, *14*, 5567–5582.
- (82) Wang, L. et al. Accurate and reliable prediction of relative ligand binding potency in prospective drug discovery by way of a modern free-energy calculation protocol and force field. *J. Am. Chem. Soc.* **2015**, *137*, 2695–2703.
- (83) Suh, D.; Radak, B. K.; Chipot, C.; Roux, B. Enhanced configurational sampling with hybrid non-equilibrium molecular dynamics-Monte Carlo propagator. *J. Chem. Phys.* **2018**, *148*, 14101.
- (84) Chen, Y.; Roux, B. Enhanced Sampling of an Atomic Model with Hybrid Nonequilibrium Molecular Dynamics-Monte Carlo Simulations Guided by a Coarse-Grained Model. *J. Chem. Theory Comput.* **2015**, *11*, 3572–3583.
- (85) Gapsys, V.; Pérez-Benito, L.; Aldeghi, M.; Seeliger, D.; van Vlijmen, H.; Tresadern, G.; de Groot, B. L. Large scale relative protein ligand binding affinities using non-equilibrium alchemy. *Chem. Sci.* **2020**, *11*, 1140–1152.
- (86) Radak, B. K.; Roux, B. Efficiency in nonequilibrium molecular dynamics Monte Carlo simulations. *J. Chem. Phys.* **2016**, *145*, 134109.
- (87) Towns, J.; Cockerill, T.; Dahan, M.; Foster, I.; Gaither, K.; Grimshaw, A.; Hazelwood, V.; Lathrop, S.; Lifka, D.; Peterson, G. D.; Roskies, R.; Scott, J. R.; Wilkins-Diehr, N. XSEDE: Accelerating Scientific Discovery. *Comput. Sci. Eng.* **2014**, *16*, 62–74.



**Table 1:** Comparison of relative hydration free energies<sup>a</sup> obtained by stepwise and concerted protocols with the original AMBER softcore potentials (labeled as "Original") and with the proposed second-order smoothstep function (labeled as SSC(2)).

Transformation	stepwise	concerted			
	Original	Original	$\Delta^b$	SSC(2)	$\Delta^b$
methane $\rightarrow$ 0	-2.34(02)	-2.34(02)	0.00	-2.36(03)	0.02
methanol $\rightarrow$ 0	3.78(02)	3.84(03)	0.06	3.85(04)	0.07
ethane $\rightarrow$ 0	-2.51(02)	-2.54(03)	0.03	-2.54(04)	0.03
toluene $\rightarrow$ 0	0.84(04)	0.80(04)	0.04	0.82(07)	0.02
neopentane $\rightarrow$ 0	-2.66(04)	-2.67(07)	0.01	-2.69(06)	0.03
2-methylfuran $\rightarrow$ 0	0.57(03)	0.56(04)	0.01	0.56(06)	0.01
2-methylindole $\rightarrow$ 0	6.25(04)	6.26(04)	0.01	6.22(08)	0.03
2-cyclopentanylindole $\rightarrow$ 0	6.59(05)	6.56(05)	0.03	6.55(09)	0.04
7-cyclopentanylindole $\rightarrow$ 0	6.85(06)	6.78(05)	0.07	6.73(10)	0.12
Avg. $\Delta$			0.03		0.04
methane $\rightarrow$ ethane	0.07(06)	0.07(08)	0.00	0.04(08)	0.03
methanol $\rightarrow$ methane	6.19(06)	6.26(07)	0.07	6.21(07)	0.02
methanol $\rightarrow$ ethane	6.19(04)	6.87(06)	0.68	6.21(04)	0.02
toluene $\rightarrow$ methane	3.23(07)	3.24(09)	0.01	3.25(10)	0.02
methane $\rightarrow$ neopentane <sup>c</sup>	0.07(14)	0.00(18)	0.07	-0.01(18)	0.08
methane $\rightarrow$ neopentane <sup>d</sup>	0.23(07)	0.20(10)	0.03	0.21(10)	0.02
2-methylfuran $\rightarrow$ methane	2.90(07)	2.95(09)	0.05	2.95(10)	0.05
2-methylindole $\rightarrow$ methane	8.66(07)	8.74(10)	0.08	8.66(12)	0.00
7-CPI <sup>e</sup> $\rightarrow$ 2-CPI <sup>f</sup>	0.04(11)	0.08(14)	0.04	0.19(16)	0.15
Avg. $\Delta$			0.11		0.04

<sup>a</sup>All free energy results were  $\Delta\Delta G$  obtained by TI, except that the data from the stepwise scheme with traditional softcore potential are obtained by BAR.  $\Delta\Delta G = \Delta G_{aq} - \Delta G_{gas}$ .

<sup>b</sup>Use the results from stepwise scheme, traditional softcore potential with BAR as the reference to show the errors with respect to the reference.

<sup>c</sup>Central mapping.

<sup>d</sup>Terminal mapping.

<sup>e</sup>7-cyclopentanylindole.

<sup>f</sup>2-cyclopentanylindole.



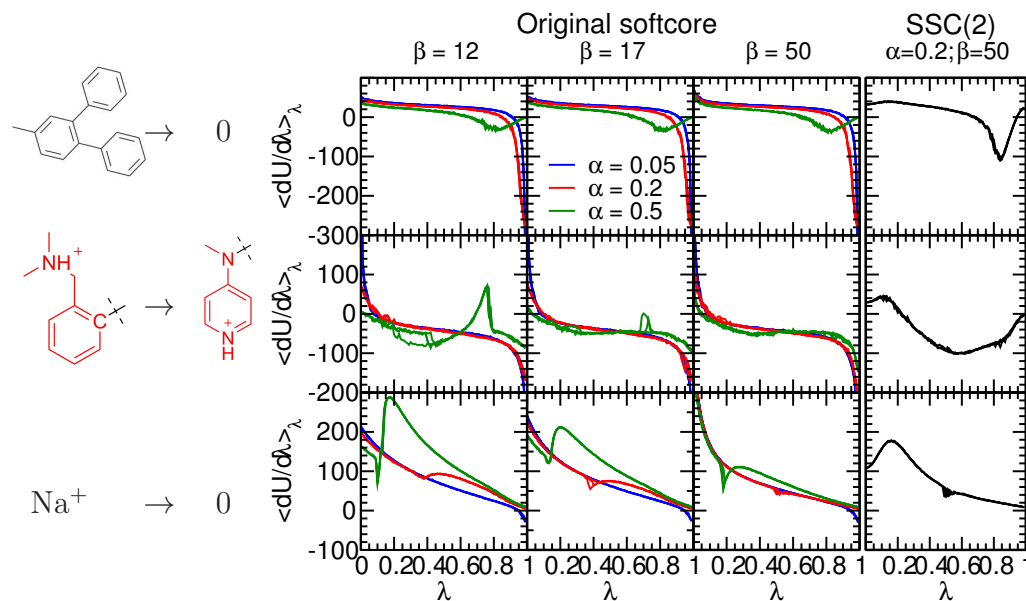


**Figure 1:** The  $\langle dU/d\lambda \rangle_\lambda$  vs.  $\lambda$  plots for alchemical simulations of three molecular systems using the one-step concerted scheme with the original AMBER softcore potential: the absolute hydration free energies for diphenyl toluene (upper rows, denoted as DPT/0) and single  $\text{Na}^+$  ion (lower rows, denoted as  $\text{Na}^+/0$ ), and the relative hydration free energy simulations for the Factor Xa ligand L51c to L51h mutation (middle rows, denoted as L51c/h). The L51c ligand has 65 atoms and L51h 58 atoms. The red-colored atoms shown are the defined softcore regions, i.e., the unique atoms for the individual ligands. The atoms common to both ligand are not shown except the connecting carbon shown in black.

The left three columns show the result using the original AMBER softcore potentials. These three columns show different  $\beta$  values ( $\text{\AA}^2$ ), and different colored curves correspond to different  $\alpha$  values (unitless).

The rightmost column shows the results from the proposed smoothstep softcore potential SSC(2) with the optimal softcore parameters ( $\alpha=12, \beta=50 \text{ \AA}^2$ ). Each curve represents one 5-ns 101-window TI simulation and there are four simulations for each condition. Note that the end-point and the large gradient-jump problems with the original softcore potentials near  $\lambda=0$  and 1 are absent in the results with the SSC(2) smoothstep softcore potentials. The particle collapse problem shown in L51c/h around  $\lambda=0.2$  to 0.4 and 0.7 to 0.8, and in  $\text{Na}^+/0$  around  $\lambda=0.2$  with the original softcore potential, also disappears in the results with the SSC(2) smoothstep softcore potentials.

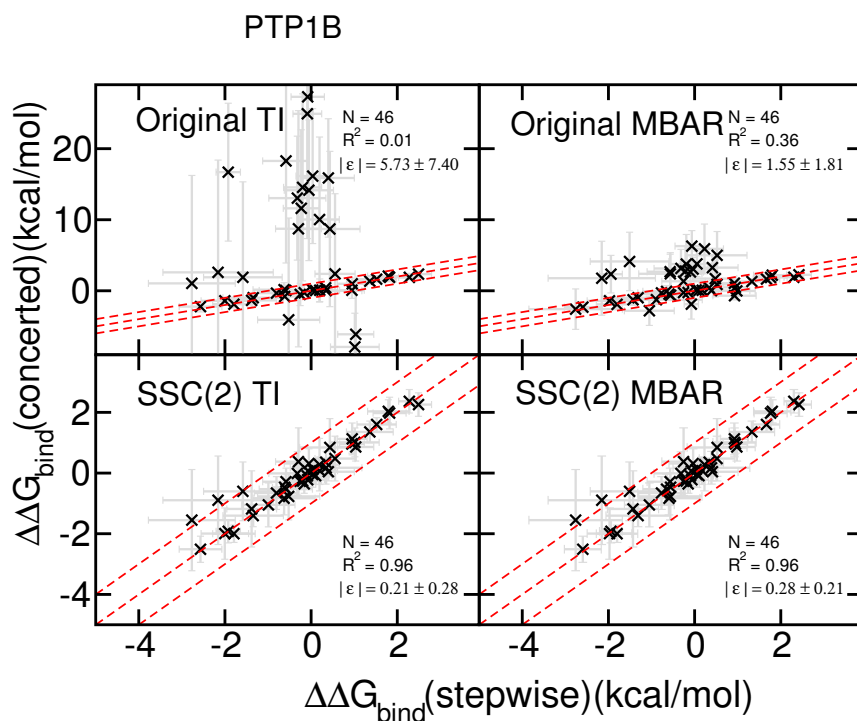


**Figure 2:** The results of RBFE of various PTP1B ligands:

Upper panels: simulations results with the original AMBER softcore potential parameter set and the linear combination of the softcore potentials, analyzed by TI (left panels) and MBAR (right panels).

Lower panels: simulations results with the proposed second order smoothstep function SSC(2) and the softcore potential parameter set ( $\alpha=0.2$ ,  $\beta=50 \text{ \AA}^2$ ), analyzed by TI (left panels) and MBAR (right panels). Plots show the comparison between the stepwise scheme (x-axis) and the concerted scheme (y-axis). The dashed red lines indicate the region of  $\pm 1.0$  kcal/mol difference.

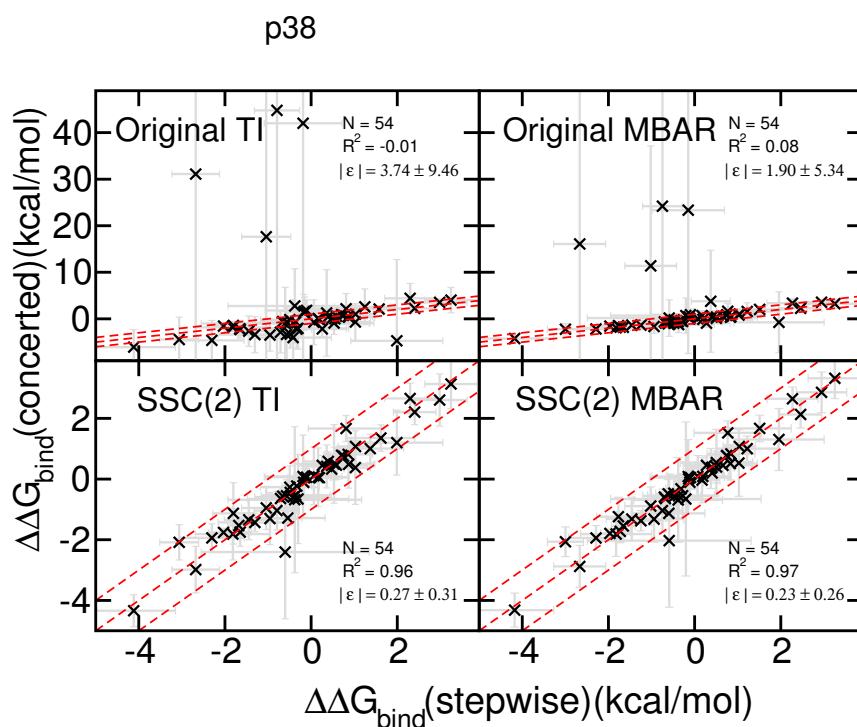


**Figure 3:** The results of RBFE of various p38 ligands:

Upper panels: simulations results with the original AMBER software potential parameter set and the linear combination of the software potentials, analyzed by TI (left panels) and MBAR (right panels).

Lower panels: simulations results with the proposed second order smoothstep function SSC(2) and the software potential parameter set ( $\alpha=0.2$ ,  $\beta=50 \text{ \AA}^2$ ), analyzed by TI (left panels) and MBAR (right panels). Plots show the comparison between the stepwise scheme (x-axis) and the concerted scheme (y-axis). The dashed red lines indicate the region of  $\pm 1.0$  kcal/mol difference.

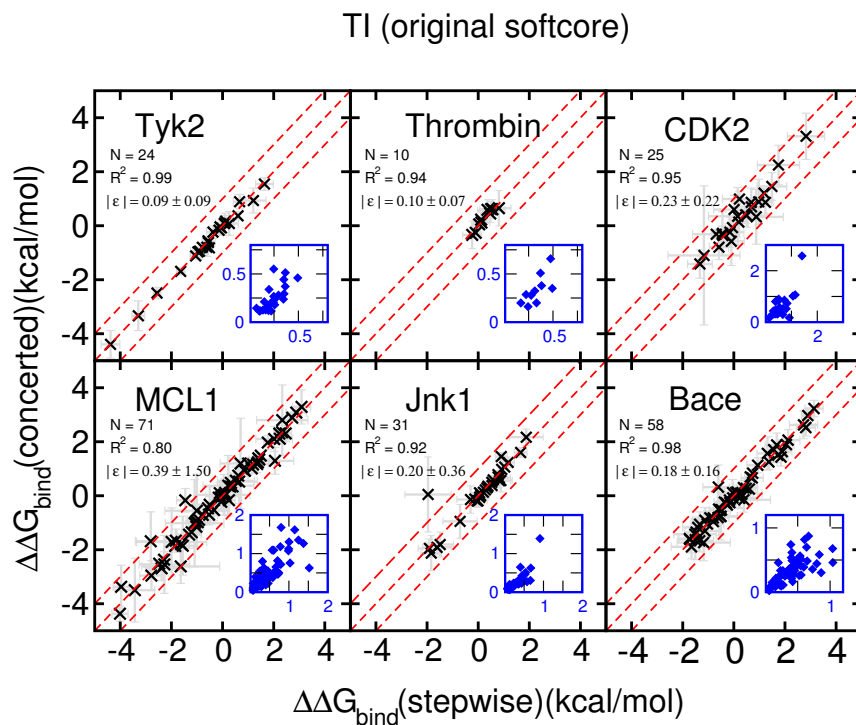


**Figure 4:** The results (y-axis) of RBF for 6 targets of the JACS data set using the concerted scheme and the AMBER original softcore potential with default parameters ( $\alpha=0.5$ ,  $\beta=12 \text{ \AA}^2$ ) are compared with corresponding values with the stepwise scheme (x-axis). The dashed red lines indicate the region of  $\pm 1.0$  kcal/mol difference. The corresponding standard deviations are plotted as gray error bars and also shown in the small blue inset plots.

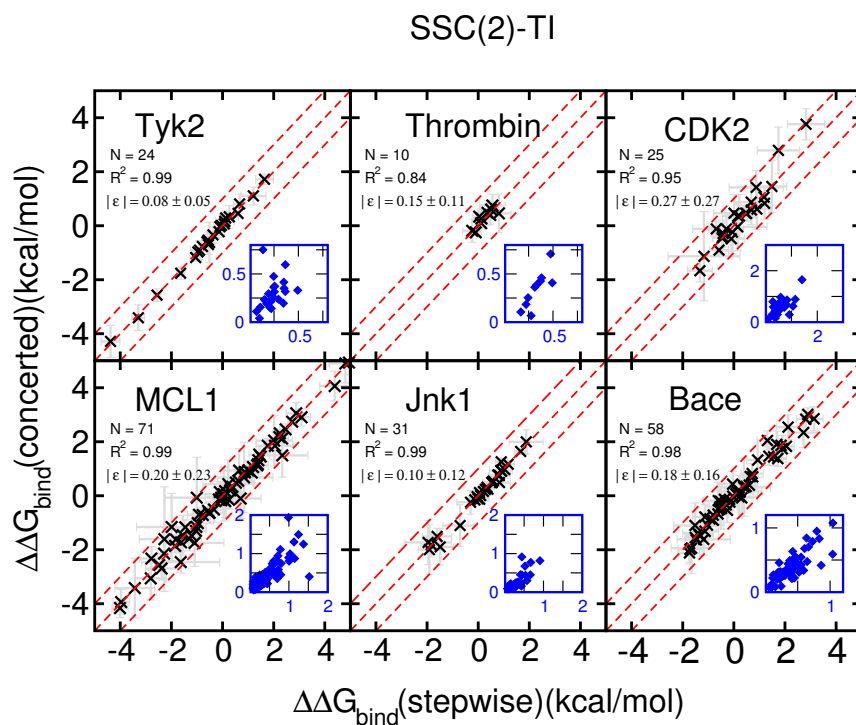


**Figure 5:** The results of RBFE for 6 targets of the JACS data set using the concerted scheme and SSC(2) smoothstep softcore potential ( $\alpha=0.2$ ,  $\beta=50 \text{ \AA}^2$ ). Plots show SSC(2) values (y-axis) compared with corresponding values with the stepwise scheme (x-axis). The dashed red lines indicate the region of  $\pm 1.0$  kcal/mol difference. The corresponding standard deviations are plotted as gray error bars and also shown in the small blue inset plots.

## Graphical TOC Entry

